catalysts

MDPI

Article

# Impact of Coordination Features of Co(II)-Glycine Complex on the Surface Sites of $Co/SiO_2$ for Fischer–Tropsch Synthesis

**Qing-Qing Hao [1,*], Min Hu [1], Zhi-Xia Xie [1], Xiaoxun Ma [1], Wei Wang [2] and Hua-Ping Ren [3,*]**

[1] School of Chemical Engineering, Northwest University, Xi'an 710069, China; humin19940426@163.com (M.H.); xiezx199605@163.com (Z.-X.X.); maxym@nwu.edu.cn (X.M.)
[2] College of Chemistry and Chemical Engineering, BaoJi University of Arts and Sciences, Baoji 721013, China; wang_wei@bjwlxy.cn
[3] School of Science, Xijing University, Xi'an 710123, China
* Correspondence: haoqq@nwu.edu.cn (Q.-Q.H.); renhuaping@xijing.edu.cn (H.-P.R.);

Received: 17 October 2020; Accepted: 4 November 2020; Published: 9 November 2020


**Abstract:** To investigate the effect of coordination features of Co(II)-glycine complex on the performance of $Co/SiO_2$ for Fischer–Tropsch (FT) synthesis, Co(II)-glycine complex precursors were prepared by the conventional method, i.e., simply adding glycine to the solution of Co nitrate and novel route, i.e., reaction of glycine with cobalt hydroxide. The $SiO_2$-supported Co catalysts were prepared by using the different Co(II)-glycine complexes. It is found that glycine is an effective chelating agent for improving the dispersion of Co and the mass-specific activity in FT synthesis when the molar ratio of glycine/$Co^{2+}$ = 3, which is independent to the preparation method in this study. Significantly, the surface Co properties were significantly influenced by the coordination features of the $Co^{2+}$ and the molar ratio of glycine to $Co^{2+}$ in the Co(II)-glycine complex. Specifically, the $Co(3gly)/SiO_2$ catalyst prepared by the novel route exhibits smaller and homogenous Co nanoparticles, which result in improved stability compared to $Co\text{-}3gly/SiO_2$ prepared by the conventional method. Thus, the newly developed method is more controllable and promising for the synthesis of Co-based catalysts for FT synthesis.

**Keywords:** Fischer–Tropsch; cobalt; dispersion; glycine; chelating

## 1. Introduction

Fischer–Tropsch (FT) synthesis is a promising process to convert syngas ($CO + H_2$) derived from non-petroleum-based resources such as coal, biomass, and natural gas to super-clean fuels and high-value-added fine chemicals [1,2]. Cobalt-based catalysts have been widely investigated for FT synthesis due to its high activity, high resistance to deactivation, low water–gas shift activity, and reasonable reservoir [3,4]. Commonly, the metallic cobalt ($Co^0$) is the active site for FT synthesis. Thus, to increase the dispersion of cobalt, cobalt precursors are generally deposited on porous oxide supports with a high surface area such as alumina, silica, or clays [5–8]. Cobalt nitrate precursor is often used owing to its high solubility allows for high metal loading in a single impregnation step. However, poor dispersions and inhomogeneous size distributions of cobalt are frequently obtained, which result in the lower mass-specific activity and higher deactivation rate [9,10]. Thus, to achieve higher mass-specific activity of Co-based catalysts, different methods have been explored to increase the cobalt dispersion, such as changing the precursor [9,11], co-impregnation with chelating agents [12–17], or modifying the drying or calcination procedure [18–20].

Among the above-mentioned methods, cobalt nitrate co-impregnation with chelating agents has been proved an effective approach to decrease the particle size of Co [13]. The essence of this

approach is to replace the $H_2O$ ligand in the $[Co(H_2O)_6(NO_3)_2]$ by organic ligand to form multidentate chelated Co ions $[Co(ligand)_x(H_2O)_{6-x}]^{2+}$ through successive complexation reactions. Thus, in the impregnation solution, the structures and coordination features of the complexes are diverse [21,22]. Moreover, it has been proved that only a part of $Co^{2+}$ in the impregnation solution participated in the complex formation with chelate agents [10,14], which is influenced by the ratio of the chelating agent to metal and the pH of the solution. Thus, varying Co species exist in the impregnation solution, which makes the drying and calcination process less controllable and results in the inhomogeneous Co oxide particles over the support due to the different thermal decomposition behavior and the interaction with the support of the Co species. Although the obtained catalysts have a higher catalytic activity, they usually exhibit a high deactivation rate due to the inhomogeneous Co particle size distributions, which leads to the sintering of small cobalt particles through Ostwald ripening [23–27]. Therefore, exploring controllable methods for the synthesis of highly dispersed Co-supported catalyst with homogenous size distribution of Co is crucial for development of high-performance FT catalysts in industry.

Glycine, as the smallest amino acid, is inexpensive and readily available, which makes it promising as a chelating agent for the synthesis of highly dispersed metal-supported catalysts [28,29]. However, the previous report demonstrated that simply adding glycine to the impregnation solution of cobalt nitrate was not effective at all and the dispersion of Co is very similar to that of $Co/SiO_2$ prepared in the absence of glycine [10,30]. The authors claim that this observation should be attributed to the lower complex formation constants of glycine with $Co^{2+}$ [30]. However, this is inconsistent with the preliminary result in our work. As mentioned above, the surface properties of Co over the supported catalysts can be significantly influenced by the coordination features of the Co(II)-glycine complexes in the impregnation solution. Thus, a detailed investigation is still needed to illuminate the impact of preparation method, coordination manner, and coordination numbers of Co(II)-glycine complex on the Co dispersion and ultimate catalytic performance in FT synthesis.

In this work, using a newly developed method, the Co(II)-glycine complexes were prepared by the reaction of glycine with cobalt hydroxide, which was used in the preparation of a $SiO_2$-supported Co catalyst. For comparison, the Co-supported catalyst was also prepared by co-impregnation with the impregnation solution containing cobalt nitrate and glycine. Consequently, the impact of preparation methods, coordination features, and coordination numbers of the Co(II)-glycine on the Co dispersion and size distribution were comparatively investigated. Contrary to the previous report, the Co catalyst prepared by co-impregnation of cobalt nitrate and glycine exhibits highly dispersed Co and higher catalytic activity in FT synthesis compared to that of $Co/SiO_2$ prepared in the absence of glycine. Significantly, the $Co(3gly)/SiO_2$ catalyst prepared from the homogenous Co complex exhibits smaller Co particle size and narrower size distribution, which results in a higher stability in the FT reaction.

## 2. Results and Discussion

### *2.1. Preparation of $SiO_2$-Supported Catalysts with Different Co(II)-Glycine Complexes*

As shown in Figure 1A, the impregnation solution containing different Co complex precursors exhibits different colors and characters. Actually, $H_2O$ is regarded as a ligand for $Co^{2+}$ in the cobalt nitrate aqueous solution. Thus, the complex in the cobalt nitrate impregnating solution can be denoted as $[Co(H_2O)_6](NO_3)_2$ (Figure 1(Aa)). In contrast, the ligand of $H_2O$ will be substituted by glycine through adding glycine to the cobalt nitrate aqueous solution (Figure 1(Ab)). However, the coordination features of Co in the solution cannot be confirmed, and thus the Co species in the solution is multiform such as $[Co(H_2O)_6](NO_3)_2$ and $[Co(glycine)_x(H_2O)_{6-2x}](NO_3)_2$ with different coordination numbers, which is related to the pH of the solution. In the case of the novel route, the Co(II)-glycine complex was prepared by the reaction of glycine with $Co(OH)_2$, which resulted in the formation of a homogenous $[Co(glycine)_2(H_2O)_2]$ complex (Figure 1(Ac)) [28,29], which is very different in terms of colors and characters compared to the impregnation solution containing Co nitrate and Co nitrate/glycine.

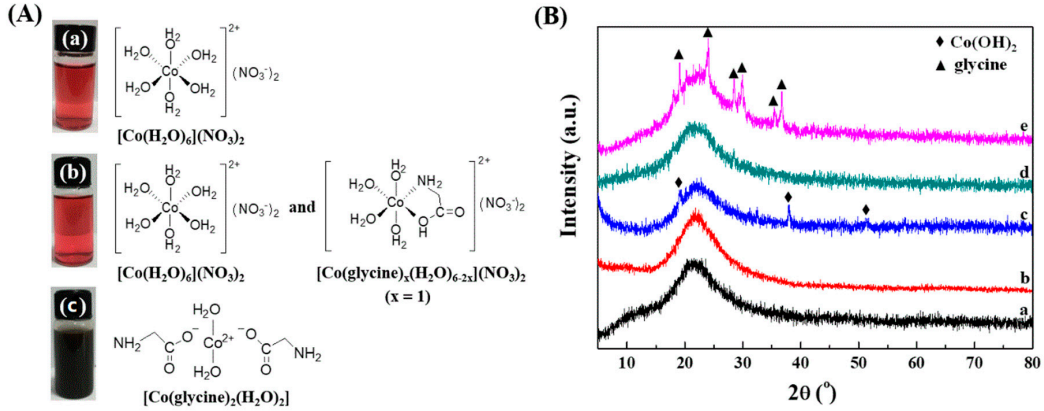


**Figure 1.** (**A**) the colors, characters, and structures of the impregnating solution of $[Co(H_2O)_6](NO_3)_2$ (**a**), $[Co(H_2O)_6](NO_3)_2$ and $[Co(glycine)_x(H_2O)_{6-2x}](NO_3)_2$ (**b**), and $[Co(glycine)_2(H_2O)_2]$ (**c**); (**B**) XRD patterns of the uncalcined catalysts for $Co/SiO_2$ (a), $Co\text{-}3gly/SiO_2$ (b), $Co(1gly)/SiO_2$ (c), $Co(3gly)/SiO_2$ (d), and $Co(5gly)/SiO_2$ (e).

After the Co complex was deposited on the $SiO_2$ support, the crystal structure of Co species over the uncalcined catalysts was investigated by XRD technique. As shown in Figure 1B, no diffraction peaks assigned to Co species are observed over $Co/SiO_2$ and $Co\text{-}3gly/SiO_2$. These observations indicate that the $[Co(H_2O)_6](NO_3)_2$ and $[Co(glycine)_x(H_2O)_{6-2x}](NO_3)_2$ is uniformly dispersed over the $SiO_2$ as a noncrystalline structure. In the case of $Co(1gly)/SiO_2$, three weak peaks at 2θ of 19.1°, 37.8°, and 51.3° assigned to the $Co(OH)_2$ phase (PDF#: 74-1057) can be observed. This indicates that not all of the $Co(OH)_2$ is coordinated by glycine when the molar ratio of glycine/$Co(OH)_2$ = 1. In contrast, as the molar ratio of glycine/$Co(OH)_2$ is increased to 3, there are no diffraction peaks assigned to Co species over the $Co(3gly)/SiO_2$, which indicates that the $Co(OH)_2$ is fully coordinated by the glycine and gives the homogenous Co complex with stable and definite structure $[Co(glycine)_2(H_2O)_2]$ on the $SiO_2$. When further increasing the molar ratio of glycine/$Co(OH)_2$ to 5, the peaks assigned to glycine (PDF# 32-1702) can be clearly seen over $Co(5gly)/SiO_2$, indicating the glycine is remarkably excessive for the formation of Co(II)-glycine complex.

The thermal decomposition behavior of different Co precursor and Co(II)-glycine complexes over the catalysts was investigated through thermal gravity (TG) measurement. From the differential thermal gravity (DTG) curves in Figure 2, the decomposition of cobalt nitrate over $Co/SiO_2$ occurs at about 188 °C. In contrast, the $Co\text{-}3gly/SiO_2$ prepared via co-impregnation with cobalt nitrate and glycine shows four mass loss stages with maximum mass loss rate at about 168, 223, 256, and 290 °C. This observation indicates that the Co species over $Co\text{-}3gly/SiO_2$ should contain multiple coordination states, that are different Co(II)-glycine coexisting over the $Co\text{-}3gly/SiO_2$ catalyst. In the case of $Co(xgly)/SiO_2$, i.e., the Co(II)-glycine complexes prepared by the reaction of $Co(OH)_2$ with glycine, the total weight loss of the catalysts is in the order of $Co(1gly)/SiO_2 < Co(3gly)/SiO_2 < Co(5gly)/SiO_2$, which is consistent with the amount of introduced glycine. The maximum mass loss rate for $Co(1gly)/SiO_2$ is about at 226 and 254 °C. Significantly, when compared to the $Co\text{-}3gly/SiO_2$, $Co(3gly)/SiO_2$ shows two mass loss stages with maximum mass loss rate at about 210 and 318 °C, which are higher than that of $Co\text{-}3gly/SiO_2$. This further indicates that the structure and coordination features of Co complexes in the $Co\text{-}3gly/SiO_2$ and $Co(3gly)/SiO_2$ prepared by different methods are significantly different with each other. For the $Co(5gly)/SiO_2$, the first weight loss stage with maximum mass loss rate at about 211 °C should be attributed to the decomposition of excess glycine. In addition, because the last weight loss stage is at about 367 °C, the calcination temperature for all of the catalysts is fixed at 400 °C.

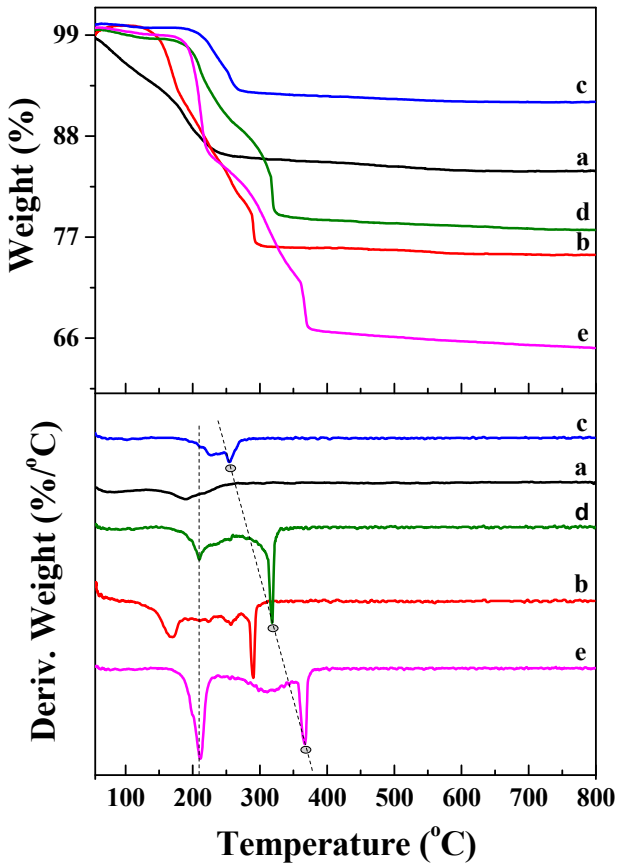


**Figure 2.** TG and DTG curves of $Co/SiO_2$ (a), $Co\text{-}3gly/SiO_2$ (b), $Co(1gly)/SiO_2$ (c), $Co(3gly)/SiO_2$ (d), and $Co(5gly)/SiO_2$ (e).

### *2.2. Textural and Structural Properties of Catalysts*

The porous structure of the catalysts was measured by $N_2$ adsorption measurement (Figure S1) and the textural properties are summarized in Table 1. As expected, the Brunauer-Emmett-Teller (BET) surface area, pore volume, and average pore size of the Co-supported catalysts are obviously decreased compared to the $SiO_2$ support due to the introduction of Co species into the pores and surface of $SiO_2$. It should be noted that the BET surface area, pore volume, and average pore size of $Co\text{-}3gly/SiO_2$ are larger than that of $Co/SiO_2$ prepared in the absence of glycine. It has been proved that the viscosity of the impregnation solution will be significantly increased upon evaporation of the solvent in the presence of chelating agents [13]. Thus, this can be applied to explain the above observations. The increased viscosity of the impregnating solution caused by the addition of glycine will suppress the outward flow of the solution and avoid blocking the pores, which leads to more uniform distribution of Co species inside the pores of the support. Moreover, the smaller $Co_3O_4$ particle size over $Co\text{-}3gly/SiO_2$ may contribute to the larger surface area. In the case of $Co(xgly)/SiO_2$, however, the BET surface area, pore volume, and average pore size are smaller than that of $Co\text{-}3gly/SiO_2$. As previously discussed, the coordination features of the Co(II)-glycine complexes prepared by different methods are very different, which result in the different viscosities and interactions with the $SiO_2$ support. Consequently, the porous structures of the catalysts prepared by different Co complexes are obviously different with each other, which will further influence the surface metallic Co site over the catalysts.

**Table 1.** Summary of the textural properties of the $SiO_2$ and catalysts.

| Catalysts | BET Surface Area ($m^2 \cdot g^{-1}$) | Pore Volume ($cm^3 \cdot g^{-1}$) | Average Pore Size (nm) |
|---|---|---|---|
| $SiO_2$ | 354.2 | 1.22 | 13.77 |
| $Co/SiO_2$ | 250.9 | 0.56 | 9.00 |
| $Co\text{-}3gly/SiO_2$ | 296.9 | 0.72 | 9.69 |
| $Co(1gly)/SiO_2$ | 207.5 | 0.47 | 7.97 |
| $Co(3gly)/SiO_2$ | 239.0 | 0.50 | 8.33 |
| $Co(5gly)/SiO_2$ | 210.7 | 0.60 | 7.97 |

The crystal structure of the Co species over the calcined catalysts was further investigated by XRD technique. As shown in Figure 3, only the $Co_3O_4$ crystal phase can be seen for all of the catalysts. However, the full width at half maximum (FWHM) of the (311) diffraction peak is obviously different, indicating the different particle size of $Co_3O_4$ over the catalysts. Indeed, the particle size of $Co_3O_4$ can be calculated by using the Scherrer formula. However, because of the relatively big error for the small crystal $Co_3O_4$ for this method, the particle size of $Co_3O_4$ is qualitatively discussed in this section. It can be concluded that the particle size of $Co_3O_4$ over the $Co\text{-}3gly/SiO_2$ and $Co(xgly)/SiO_2$ catalysts prepared in the presence of glycine is remarkably smaller than that of $Co/SiO_2$ prepared using cobalt nitrate as a precursor. In the case of $Co(xgly)/SiO_2$, the particle size of $Co_3O_4$ is decreased with increasing the molar ratio of glycine to $Co(OH)_2$. The Co particle size for the reduced catalysts was investigated by using TEM and $H_2$ chemisorption in Section 3.3. In addition, it must be pointed out that the formation of the $Co_2SiO_4$ phase cannot be detected by XRD because the peak of the $Co_2SiO_4$ is overlapped with that of the $Co_3O_4$ [31].

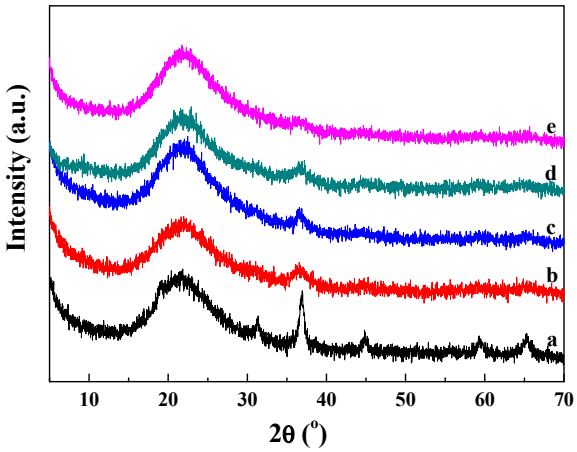


**Figure 3.** XRD patterns of the calcined catalysts for $Co/SiO_2$ (a), $Co\text{-}3gly/SiO_2$ (b), $Co(1gly)/SiO_2$ (c), $Co(3gly)/SiO_2$ (d), and $Co(5gly)/SiO_2$ (e).

The surface Co species over the calcined catalysts was further identified by XPS measurements based on the chemical shift of the binding energy and the results are shown in Figure 4. For the $Co/SiO_2$ catalyst, the Co $2p_{3/2}$ peak is observed at 779.8 eV, which is slightly higher than the binding energy of the pure $Co_3O_4$ phase (778.5 eV) reported in the literature [30] owing to the interaction between the smaller $Co_3O_4$ particles and the $SiO_2$ support. In contrast, the Co $2p_{3/2}$ peak over $Co\text{-}3gly/SiO_2$ is almost invisible (all the samples were tested two times to verify the validity of the result). However, $Co\text{-}3gly/SiO_2$ exhibits clear peaks of $Co_3O_4$ from the XRD result. These observations indicate that the distribution of $Co_3O_4$ particles throughout the $SiO_2$ particles was not homogeneous over $Co\text{-}3gly/SiO_2$. As previously discussed, the addition of glycine will increase the viscosity of the impregnating solution, which can suppress the outward flow of the solution and leads to the small amount of Co species located at the external surface of the support. In the case of $Co(xgly)/SiO_2$,

the obvious characteristic is that the binding energy of the Co species is higher than that of the $Co/SiO_2$ catalyst. Based on the literature, the binding energy of the Co $2p_{3/2}$ peak of $Co_2SiO_4$ is about 781.5 eV [29]. Thus, the higher binding energy of the Co $2p_{3/2}$ peak over $Co(3gly)/SiO_2$ (781.6 eV) indicates the formation of $Co_2SiO_4$-like species over these catalysts due to the smaller Co oxide particle size. In addition, it is worth noting that the binding energy of the Co $2p_{3/2}$ peak of $Co(1gly)/SiO_2$ (782.6 eV) is clearly higher than that of $Co(3gly)/SiO_2$ (781.6 eV). As revealed from the XRD result, the $Co(OH)_2$ exists over the $Co(1gly)/SiO_2$ catalyst. Thus, the higher binding energy of the Co $2p_{3/2}$ peak of $Co(1gly)/SiO_2$ is attributed to the formation of $Co_2SiO_4$ because $Co_2SiO_4$ can be easily formed via the reaction of $Co(OH)_2$ with $SiO_2$ support [31]. In addition, similar with the $Co\text{-}3gly/SiO_2$, the Co $2p_{3/2}$ peak over $Co(5gly)/SiO_2$ is very weak, indicating decreased Co/Si surface ratios. We speculate that the uncombined glycine over $Co\text{-}3gly/SiO_2$ and $Co(5gly)/SiO_2$ may induce the silica migration, and coating or encapsulation of the $CoO_x$ species in the process of drying and calcination [32].

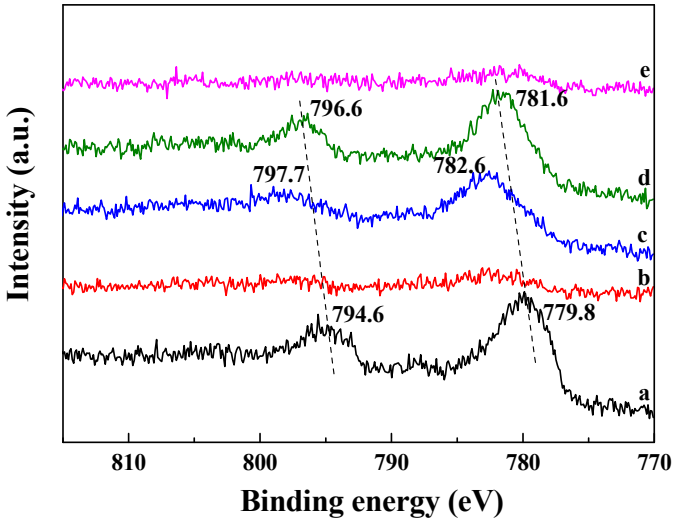


**Figure 4.** XPS spectra in the Co 2p region of the calcined $Co/SiO_2$ (a), $Co\text{-}3gly/SiO_2$ (b), $Co(1gly)/SiO_2$ (c), $Co(3gly)/SiO_2$ (d), and $Co(5gly)/SiO_2$ (e).

### *2.3. Co Particle Size and Reduction Behavior of the Catalysts*

$H_2$-TPR measurement was used to evaluate the reduction behavior of the catalysts (Figure 5). The $Co/SiO_2$ show two discrete peaks at about 296 and 350 °C, which are assigned to the two-step reduction of $Co_3O_4$ to CoO and CoO to metallic Co, respectively. In addition, the $Co/SiO_2$ shows a weakly broad peak from 500 to 800 °C, which can be assigned to the reduction of the Co species having a stronger interaction with $SiO_2$. In contrast, the $H_2$-TPR profile of the $SiO_2$-supported Co catalysts prepared with the glycine-assisted method show similar and clear high temperature reduction peaks at a temperature range of 650 to 900 °C, which are attributed to the reduction of the $Co_2SiO_4$-like species. However, the reduction behavior of the Co species are significantly influenced by the preparation method of Co(II)-glycine complexes and the molar ratio of glycine to $Co(OH)_2$. In order to quantitatively evaluate the reduction degree of cobalt over the catalysts, the $O_2$ pulse titration is carried out and the results are listed in Table 2. The reduction degree of the catalyst prepared in the presence of glycine is obviously lower than that of $Co/SiO_2$ (52.9%). Moreover, the reduction degree of $Co\text{-}3gly/SiO_2$ is higher than that of $Co(xgly)/SiO_2$. For $Co(xgly)/SiO_2$, as the molar ratio of glycine to $Co(OH)_2$ is increased, the reduction degree of the catalysts decrease correspondingly.

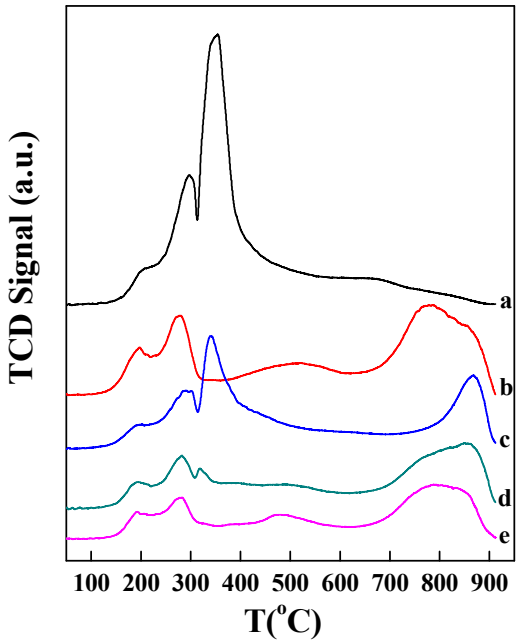


**Figure 5.** $H_2$-TPR profiles for $Co/SiO_2$ (a), Co-3gly/$SiO_2$ (b), Co(1gly)/$SiO_2$ (c), Co(3gly)/$SiO_2$ (d), and Co(5gly)/$SiO_2$ (e).

**Table 2.** Summarized cobalt properties over different catalysts.

| Catalysts | Co Size (nm) | | Reduction Degree [a] (%) | Co Dispersion [b] (%) | Surface Co Density ($10^{-2}$ mmol/$g_{cat}$) |
|---|---|---|---|---|---|
| | $d(Co)_{TEM}$ | $d(Co)_H$ [c] | | | |
| $Co/SiO_2$ | 7.2 | 9.4 | 52.9 | 5.4 | 6.4 |
| Co-3gly/$SiO_2$ | 4.0 | 3.4 | 38.3 | 10.9 | 13.0 |
| Co(1gly)/$SiO_2$ | — | 7.9 | 28.7 | 3.5 | 4.2 |
| Co(3gly)/$SiO_2$ | 2.5 | 2.4 | 21.3 | 8.5 | 10.1 |
| Co(5gly)/$SiO_2$ | — | 2.1 | 16.7 | 7.8 | 9.3 |

[a] Determined from $O_2$-pulse titration; [b] determined from $H_2$-chemisorption; [c] calculated using Co dispersion and reduction degree.

Commonly, the surface $Co^0$ density (Co dispersion) of the catalyst is determined by the particle size and the reduction degree of Co. $H_2$-chemisorption is an effective technique to obtain the actual surface $Co^0$ density and the dispersion (normalized by the total moles of Co over the catalyst). As shown in Table 2, the Co dispersion of Co-3gly/$SiO_2$ (10.9%) is two-times higher than that of $Co/SiO_2$ (5.4%). This is higher than the result reported by Koizumi et al. [30], in which the dispersion of Co over the catalyst (5 wt.% Co loading) prepared through the co-impregnation of Co nitrate and glycine is almost similar (about 4.9%) with that of $Co/SiO_2$ prepared in the absence of glycine. Through comparing the preparation process of the catalyst in the literature and our work, we can found that aqueous $NH_3$ solution was added to the impregnation solution to maintain the pH at 9–10 in their work, while the pH of the impregnation solution was not regulated in our work. Thus, the distinct difference of the Co dispersion between the two works may be caused by the different pH of the impregnation solution, which may result in the different coordination features of Co(II)-glycine. These observations also proved that the coordination features and the microenvironment of the Co species have prominently impacted on the Co oxide properties over the catalyst after calcination. Moreover, the Co(3gly)/$SiO_2$ shows the highest the Co dispersion in the three catalysts prepared by the novel method. The $Co^0$ particle size of the reduced catalysts was calculated from the dispersion and the reduction degree of Co. As expected, the $Co/SiO_2$ shows the largest $Co^0$ particle size (9.4 nm). In contrast, the $Co^0$ particle size over the Co-3gly/$SiO_2$ is obviously decreased owing to the introduction of glycine. For the Co(*x*gly)/$SiO_2$, the $Co^0$ particle size is continuously decreased with increasing of the molar ratio of

glycine to $Co(OH)_2$. However, the $Co^0$ particle size over $Co(1gly)/SiO_2$ (7.9 nm) is much larger than $Co(3gly)/SiO_2$ and $Co(5gly)/SiO_2$. As revealed from the XRD result, the $Co(OH)_2$ phase was detected over the uncalcined $Co(1gly)/SiO_2$. Moreover, the lower ratio of glycine to Co will decrease the capsulate effect of glycine. Thus, the bigger $Co^0$ particle size over $Co(1gly)/SiO_2$ can be attributed to the two above-mentioned factors. Correspondingly, the smaller $Co^0$ particle size over $Co(3gly)/SiO_2$ and $Co(5gly)/SiO_2$ can be attributed to the stronger capsulate effect of the coordinate glycine around the $Co^{2+}$ [33–35].

Moreover, the $Co^0$ particle sizes over the reduced $Co/SiO_2$, $Co\text{-}3gly/SiO_2$, and $Co(3gly)/SiO_2$ were also examined via HAADF-STEM technique to further study the effect of coordination features of Co complex on the size distribution of $Co^0$ particles. As shown in Figure 6, the $Co^0$ particles' size over the $Co/SiO_2$ is distributed in the wide range of 3.5–11.5 nm. In contrast, the particle size of $Co^0$ over $Co\text{-}3gly/SiO_2$ is clearly decreased, and the size distribution of the $Co^0$ particles is in the range of 2.3–6.3 nm. Significantly, the size distribution of the $Co^0$ particles is very homogenous and further narrowed in the range of 2–3 nm. These observations indicate that the prepared method and the coordination features of the Co complex have remarkable influence on the size distribution of the $Co^0$ particles.

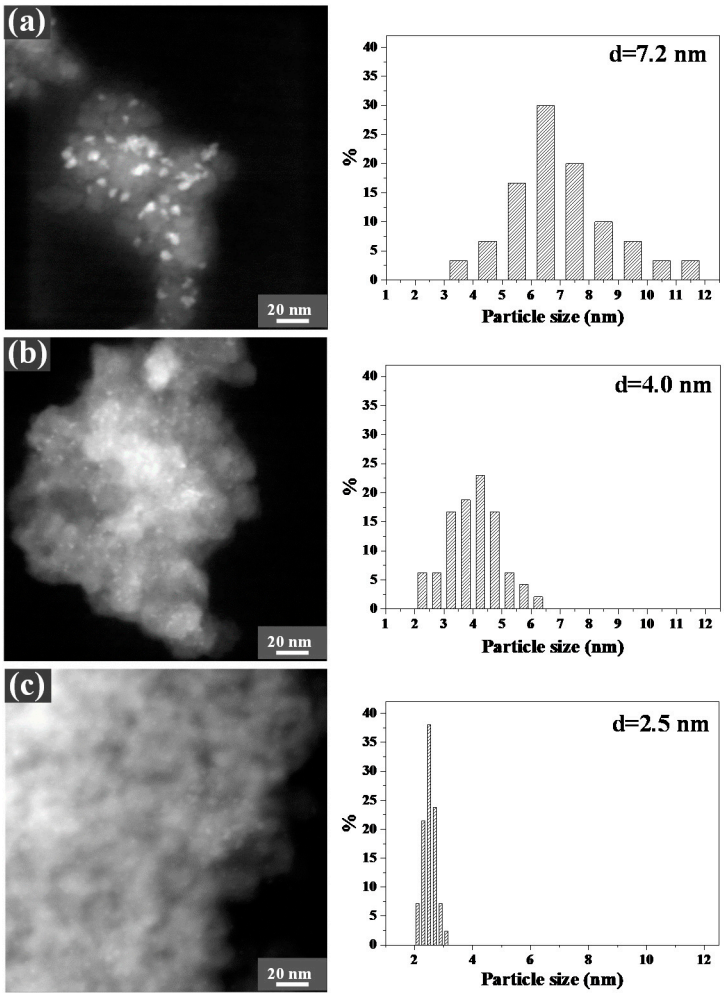


**Figure 6.** HAADF-STEM images and particle size distributions of Co over the reduced catalyst of $Co/SiO_2$ (**a**), $Co\text{-}3gly/SiO_2$ (**b**), and $Co(3gly)/SiO_2$ (**c**).

### *2.4. FT Performance*

The catalysts were evaluated for FT synthesis under the conditions of 235 °C, 1 MPa, $H_2/CO = 2$, and W/F = 5.02 g h $mol^{-1}$. As shown in Figure 7, the catalytic activity (CO conversion) and stability are obviously different with each other. The CO conversions at steady state over the catalysts are increased in the order of Co-3gly/$SiO_2$ > Co(3gly)/$SiO_2$ > Co(5gly)/$SiO_2$ ≈ Co/$SiO_2$ > Co(1gly)/$SiO_2$, which is consistent with the changing trend of $Co^0$ dispersion and surface $Co^0$ density (Table 2). It should be noted that the deactivation rate of Co-3gly/$SiO_2$ is obviously higher than that of the others. In contrast, the CO conversion over Co(3gly)/$SiO_2$ is almost unchanged within the reaction time of 10 h. As revealed from the TEM result, the Co(3gly)/$SiO_2$ exhibits homogenous particle size distribution of Co. Based on the theoretical calculation, the Ostwald ripening rate could be significantly suppressed by preparing the homogeneously distributed metal particles with identical size [22]. Thus, the different stability of the two catalysts can be reasonably explained by the size distribution of Co particles over the Co-3gly/$SiO_2$ and Co(3gly)/$SiO_2$ catalysts. Moreover, for the catalysts prepared by the second method, with an increasing molar ratio of glycine/$Co^{2+}$, the CO conversion is firstly increased, and then clearly decreased. As a result, the highest CO conversion is achieved over Co(3gly)/$SiO_2$. Thus, we can conclude that the activity of the catalyst prepared in the presence of chelating agent is not only influenced by the intrinsic properties of the chelating agent, but also influenced by the ratio of chelating agent to metal ion. Moreover, from the cobalt-time-yield (CTY) in Figure 7B, the mass-specific activity of the Co-3gly/$SiO_2$ and Co(3gly)/$SiO_2$ catalysts was significantly improved, although the reduction degrees of Co over these two catalysts are lower than that of Co/$SiO_2$. However, based on the previous report [30], unfortunately, using the easily available glycine as a chelating agent is almost ineffective for improving mass-specific activity of the Co catalyst. The different results may be caused by the different pH of the impregnation solution, which leads to the different coordination features of Co.

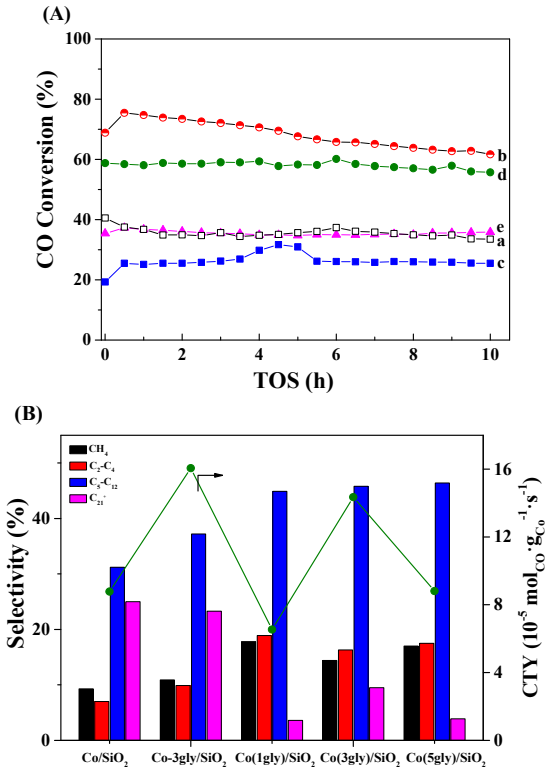


**Figure 7.** Time-on-stream CO conversion (**A**) and product selectivity (**B**) over Co/$SiO_2$ (a), Co-3gly/$SiO_2$ (b), Co(1gly)/$SiO_2$ (c), Co(3gly)/$SiO_2$ (d), and Co(5gly)/$SiO_2$ (e).

Figure 7B shows the product selectivity of the FT synthesis over these catalysts. The selectivity of $CH_4$ and $C_2$-$C_4$ over Co-3gly/$SiO_2$ is slightly increased and the selectivity of $C_{21}^+$ is slightly decreased compared to that of Co/$SiO_2$. However, in comparison with Co/$SiO_2$, the selectivity of $CH_4$ and $C_2$-$C_4$ over Co(3gly)/$SiO_2$ is significantly increased, while the selectivity of $C_{21}^+$ is significantly decreased. Based on the previous report, the surface hydrogen coverage is increased with decreasing Co particle size over the catalysts with average $Co^0$ particles smaller than 6 nm [36,37]. Thus, the above results about the product selectivity over the Co-3gly/$SiO_2$ and Co(3gly)/$SiO_2$ can be explained according to the decreased particle size of the $Co^0$ over the catalysts. In addition, the product distributions over the three catalysts prepared by the second manner are very similar to each other. The highest selectivity of $C_{21}^+$ over Co(3gly)/$SiO_2$ should be attributed to the higher CO conversion. From the above discussion about the catalytic performance, we can conclude that glycine is an effective chelating agent to improve the dispersion of Co and the mass-specific activity of Co catalysts in Fischer–Tropsch synthesis independent of the preparation method used in this study, although the reduction degree of Co is very low compared to the Co/$SiO_2$ prepared in the absence of glycine. However, the size distribution of Co and the stability in the FT synthesis was significantly influenced by the coordination features (preparation method) of the Co(II) complexes. Moreover, it should be pointed that the higher selectivity of light hydrocarbons ($C_1$-$C_4$) over the Co(3gly)/$SiO_2$ is not desirable, which makes the FT synthesis process inefficient. Thus, the preparation of the Co catalyst using glycine as a chelating agent still needs optimized.

## 3. Materials and Methods

### *3.1. Materials*

$Co(NO_3)_2{\cdot}6H_2O$ (98.5%), glycine (99%), and sodium hydroxide (NaOH, 96%) were purchased from Sinopharm Chemical Reagent Co. Ltd. (Shanghai, China)The catalyst support $SiO_2$ (Q-15) used in this study was purchased from Fuji Silysia Chemical Ltd. (Kasugai Aichi, Japan)

### *3.2. Preparation of Catalyst*

The conventional Co/$SiO_2$ catalyst was prepared from the impregnation solution containing only Co nitrate by incipient wetness impregnation method (control experiment). The $SiO_2$-supported Co catalysts using Co(II)-glycine as the precursor were prepared by two different methods: (1) the Co(II)-glycine precursor in the first method was prepared by directly adding the glycine to the solution of Co nitrate with a molar ratio of glycine/$Co^{2+}$ = 3. Then the $SiO_2$-support Co catalyst was prepared from the impregnation solution containing both Co nitrate and glycine, and this catalyst was denoted as Co-3gly/$SiO_2$; (2) the Co(II)-glycine precursors in the second method were prepared by the reaction of glycine with $Co(OH)_2$ with a different molar ratio of glycine to $Co(OH)_2$ (glycine/$Co(OH)_2$ = 1, 2, and 3). Typically, the $Co(OH)_2$ was prepared by the reaction of $Co(NO_3)_2$ with NaOH using the molar ration of $OH^-/CO^{2+}$ = 2. After the formation of the $Co(OH)_2$ precipitate, the $Co(OH)_2$ was recovered by filtration and thoroughly washing with deionized water, and then the wet $Co(OH)_2$ were dried at 80 °C for 12 h. For the preparation of the Co(II)-glycine complex, the $Co(OH)_2$ powder was slowly added to the 0.2 mol/L glycine aqueous solution at 80 °C, in which the molar ratio of glycine to $Co(OH)_2$ was 1, 3, or 5. After the addition of $Co(OH)_2$ powder, the solution was continuously stirred for 2 h at 80 °C. Finally, the $SiO_2$ powder was impregnated with the obtained solution containing Co(II)-glycine complex. These kind of catalysts were denoted as Co-*x*gly/$SiO_2$ where x = molar ratio of glycine to $Co(OH)_2$. All the catalysts were dried at 100 °C for 12 h, and then calcined at 400 °C for 4 h. The metallic Co loading for all of the catalysts was 7 wt.%.

### *3.3. Characterizations*

XRD measurement was performed on an X-ray diffractometer (D8 Advance) with Cu Kα radiation operated at 40 kV and 40 mA. The speed of scanning was 4°/min with a step size of 0.02°.

Low temperature $N_2$ adsorption was performed at −196 °C using BelSorp-Max (Bel Japan Inc., Osaka, Japan). The samples were outgassed at 300 °C for 12 h. The specific surface area was calculated by the BET method. The pore size distributions were obtained from the BJH method using adsorption branch. Thermogravimetric (TG) measurement was carried out on a Q1000DSC thermogravimetric analyzer. The uncalcined catalysts were heated from room temperature to 800 °C at a heating rate of 10 °C/min in an air atmosphere. X-ray photoelectron spectroscopy (XPS) analyses were carried out on an Axis Ultra spectrometer (Kratos Analytical Ltd., Manchester, UK) using an Al monochromatic X-ray source (Al Ka = 1486.6 eV). The C1s binding energy of adventitious carbon (284.8 eV) was taken as an internal standard for correcting any charge-induced peak shifts. The $H_2$-TPR was carried out on a BELCAT II (MicrotracBEL) instrument. The catalysts, 0.05 g, were first purged in a flow of argon at 200 °C for 30 min. After the temperature was decreased to 35 °C, the catalysts were heated to 900 °C at a heating rate of 10 °C/min under 10 vol.% hydrogen–argon mixtures with a flow rate of 30 $cm^3$/min. The reduction degree of cobalt was determined by $O_2$ pulse titration method. Firstly, about 0.1 g of catalyst was reduced in situ for 6 h at 500 °C using pure hydrogen. Afterwards, the temperature of the sample was decreased to 400 °C, and flushed with pure Ar for 1 h. At the same temperature, 3 vol.% $O_2$ was injected with pulse mode to oxidize the reduced catalyst. The reduction degree (RD, %) of the catalyst was estimated based on the consumption of oxygen assuming that metallic Co was converted to $Co_3O_4$. $H_2$-chemisorption measurements were performed on a Micromeretics ASAP 2020C instrument to evaluate the Co dispersion. Before measurement, the sample was reduced on the analysis station in situ in flowing $H_2$ at 500 °C for 6 h. Afterwards, the temperature was decreased to 100 °C and the $H_2$-chemisorption was measured at this temperature. The $H_2$ uptakes and Co dispersion (D, %) were determined using the method reported in the literature [30], assuming hemispherical geometry of the metallic Co, with surface atomic density of 14.6 atoms/$nm^2$. The particle sizes of $Co^0$ were calculated using $d(Co)_H = 96 \times RD/D$ formula. TEM micrographs were obtained on an FEI Tecnai G2 F20 S-TWIN at an acceleration voltage of 200 kV. Prior to measurement, the catalysts were reduced at 500 °C for 6 h in hydrogen, then passivated by 1% $O_2$ in argon for 1 h at room temperature.

### *3.4. Catalytic Reactions*

The catalytic performances of the catalysts in FT synthesis were tested in a fixed-bed reactor. Typically, 0.5 g of catalyst (40–60 mesh diluted with quartz sands) was firstly reduced in situ in a flow of pure $H_2$ (50 $cm^3$/min) at 500 °C for 6 h. Then the temperature was decreased to 190 °C and the syngas ($H_2$/CO = 2, 4% Ar as an internal standard) was fed into reactor. The reaction conditions were at 235 °C, 1.0 MPa, and W/F = 5.0 g·h·$mol^{-1}$. In order to prevent condensation of the products, the pipeline from the outlet of the reactor to the inlet of the gas chromatography (GC) was heated at 180 °C. The hydrocarbons in the effluent were analyzed online by GC with an HP-PONA capillary column (0.20 mm × 50 m, 0.5 μm) and a flame ionization detector (FID) (SP-3420A, Beijing Beifen-Ruili Analytical Instrument (Group) Co., Ltd. Beijing, China). The CO, $CH_4$, Ar, and $CO_2$ in the effluent were analyzed online by GC with a packed activated-carbon column and a TCD detector (SP-3420A). The selectivity for hydrocarbons was calculated on the basis of carbon number.

## 4. Conclusions

In summary, $SiO_2$-supported Co catalysts were prepared from Co(II)-glycine complex with different coordination features obtained by two different methods. It is found that glycine is an effective chelating agent to improve the dispersion of Co and the mass-specific activity of Co catalysts in Fischer–Tropsch synthesis independent of the preparation method used in this study. The characterization results revealed that the dispersion, particle size distribution, and reduction degree of Co are significantly influenced by the preparation method of Co(II)-glycine complex and the ratio of glycine/$Co^{2+}$. In comparison to the Co-3gly/$SiO_2$ prepared by the traditional co-impregnation method, the Co(3gly)/$SiO_2$ prepared by the newly developed method exhibits smaller Co particle size and homogenous size distribution of Co. The mass-specific activity of the Co-based catalyst in the FT

synthesis is significantly increased when the glycine/$Co_2^+$ = 3. However, the stability of Co(3gly)/$SiO_2$ is evidently improved compared to Co-3gly/$SiO_2$, which is attributed to the homogeneously distributed Co particles with identical size. Thus, the newly developed method is more controllable and promising for the synthesis of Co-based catalysts for FT synthesis.

**Supplementary Materials:** The following are available online at http://www.mdpi.com/2073-4344/10/11/1295/s1, Figure S1: $N_2$ adsorption-desorption isotherms and BJH pore size distribution of the catalysts.

**Author Contributions:** Q.-Q.H. and H.-P.R. conceived and designed the experiments. M.H., Z.-X.X., and W.W. carried out the experiments, the structural characterizations, and the catalytic performance test. M.H., Q.-Q.H., X.M., and H.-P.R. cowrote the manuscript, and Q.-Q.H. and. H.-P.R. finalized the manuscript. All authors have read and agreed to the published version of the manuscript.

**Funding:** This research was funded by the National Natural Science Foundation of China (No. 21406179 and 29178233), the China Postdoctoral Science Foundation (No. 2016M600810 and 2017T100767), the Natural Science Basic Research Plan in Shaanxi Province of China (No. 2019JM-054), the Scientific Research Program of Shaanxi Provincial Education Department (No. 19JC039), and the Scientific Research Project of Xi'an Science and Technology Bureau (No. 2020KJRC0113).

**Conflicts of Interest:** The authors declare no conflict of interest.

## References

1. Zhang, Q.; Kang, J.; Wang, Y. Development of novel catalysts for Fischer-Tropsch synthesis: Tuning the product selectivity. *ChemCatChem* **2010**, *2*, 1030–1058. [CrossRef]
2. Chen, Q.P.; Tian, Y.; Lyu, S.S.; Zhao, N.; Ma, K.; Ding, T.; Jiang, Z.; Wang, L.H.; Zhang, J.; Zheng, L.R.; et al. Confined small-sized cobalt catalysts stimulate carbon-chain growth reversely by modifying ASF law of Fischer-Tropsch synthesis. *Nat. Commun.* **2018**, *9*, 3250–3258. [CrossRef] [PubMed]
3. Khodakov, A.Y.; Chu, W.; Fongarland, P. Advances in the development of novel cobalt Fischer-Tropsch catalysts for synthesis of long-chain hydrocarbons and clean fuels. *Chem. Rev.* **2007**, *107*, 1692–1744. [CrossRef] [PubMed]
4. Qi, Z.Y.; Chen, L.N.; Zhang, S.C.; Su, J.; Somorjai, G.A. A Mini review of cobalt-based nanocatalyst in Fischer-Tropsch synthesis. *Appl. Catal. A Gen.* **2020**, *602*, 117701. [CrossRef]
5. Van de Water, L.G.A.; Bezemer, G.L.; Bergwerff, J.A.; Versluijs-Helder, M.; Weckhuysen, B.M.; De Jong, K.P. Spatially resolved UV-vis microspectroscopy on the preparation of alumina-supported Co Fischer-Tropsch catalysts: Linking activity to Co distribution and speciation. *J. Catal.* **2016**, *242*, 287–298. [CrossRef]
6. Girardon, J.S.; Quinet, E.; Griboval-Constant, A.; Chernavskii, P.A.; Gengembre, L.; Khodakov, A.Y. Cobalt dispersion, reducibility, and surface sites in promoted silica-supported Fischer-Tropsch catalysts. *J. Catal.* **2007**, *248*, 143–157. [CrossRef]
7. Shi, L.; Zeng, C.Y.; Lin, Q.H.; Lu, P.; Niu, W.Q.; Tsubaki, N. Citric acid assisted one-step synthesis of highly dispersed metallic Co/$SiO_2$ without further reduction: As-prepared Co/$SiO_2$ catalysts for Fischer–Tropsch synthesis. *Catal. Today* **2014**, *228*, 206–211. [CrossRef]
8. Hao, Q.-Q.; Liu, Z.-W.; Zhang, B.; Wang, G.-W.; Ma, C.; Frandsen, W.; Li, J.; Liu, Z.-T.; Hao, Z.; Su, D. Porous montmorillonite heterostructures directed by a single alkyl ammonium template for controlling the product distribution of Fischer-Tropsch synthesis over cobalt. *Chem. Mater.* **2012**, *24*, 972–974. [CrossRef]
9. Sun, S.L.; Tsubaki, N.; Fujimoto, K. The reaction performances and characterization of Fischer-Tropsch synthesis Co/$SiO_2$ catalysts prepared from mixed cobalt salts. *Appl. Catal. A Gen.* **2000**, *202*, 121–131. [CrossRef]
10. Mochizuki, T.; Hara, T.; Koizumi, N.; Yamada, M. Surface structure and Fischer-Tropsch synthesis activity of highly active Co/$SiO_2$ catalysts prepared from the impregnating solution modified with some chelating agents. *Appl. Catal. A Gen.* **2007**, *317*, 97–104. [CrossRef]
11. Girardon, J.S.; Lermontov, A.S.; Gengembre, L.; Chernavskii, P.A.; Griboval-Constant, A.; Khodakov, A.Y. Effect of Cobalt Precursor and Pretreatment conditions on the structure and Patalytic Performance of cobalt Silica-Supported Fischer-Tropsch catalyst. *J. Catal.* **2005**, *230*, 339–352. [CrossRef]
12. Mochizuki, T.; Hara, T.; Koizumi, N.; Yamada, M. Novel preparation method of highly active Co/$SiO_2$ catalyst for Fischer-Tropsch synthesis with chelating agents. *Catal. Lett.* **2007**, *113*, 165–169. [CrossRef]

13. Jos van Dillen, A.; Terörde, R.J.A.M.; Lensveld, D.J.; Geus, J.W.; de Jong, K.P. Synthesis of supported catalysts by impregnation and drying using aqueous chelated metal complexes. *J. Catal.* **2003**, *216*, 257–264. [CrossRef]
14. Koizumi, N.; Ibi, Y.; Hongo, D.; Hamabe, Y.; Suzuki, S.; Hayasaka, Y.; Shindo, T.; Yamada, M. Mechanistic aspects of the role of chelating agents in enhancing Fischer-Tropsch synthesis activity of $Co/SiO_2$ catalyst: Importance of specific interaction of Co with chelate complex during calcination. *J. Catal.* **2012**, *289*, 151–163. [CrossRef]
15. Hong, J.P.; Marceau, E.; Khodakov, A.Y.; Griboval-Constant, A.; Fontaine, C.L.; Villain, F.; Briois, V.; Chernavskii, P.A. Impact of Sorbitol addition on the structure and performance of silica-supported cobalt catalysts for Fischer-Tropsch synthesis. *Catal. Today* **2011**, *175*, 528–533. [CrossRef]
16. Bambal, A.S.; Guggilla, V.S.; Kugler, E.L.; Gardner, T.H.; Dadyburjor, D.B. Poisoning of a silica-supported cobalt catalyst due to presence of sulfur impurities in syngas during Fischer-Tropsch synthesis: Effects of chelating agent. *Ind. Eng. Chem. Res.* **2014**, *53*, 5846–5857. [CrossRef]
17. Shi, L.; Tao, K.; Kawabata, T.; Shimamura, T.; Zhang, X.J.; Tsubaki, N. Surface impregnation combustion method to prepare nanostructured metallic catalysts without further reduction: As-burnt $Co/SiO_2$ catalysts for Fischer-Tropsch synthesis. *ACS Catal.* **2011**, *1*, 1225–1233. [CrossRef]
18. Munnik, P.; Krans, N.A.; de Jongh, P.E.; de Jong, K.P. Effects of drying conditions on the synthesis of $Co/SiO_2$ and $Co/Al_2O_3$ Fischer-Tropsch catalysts. *ACS Catal.* **2014**, *4*, 3219–3226. [CrossRef]
19. Munnik, P.; de Jongh, P.E.; de Jong, K.P. Control and impact of the nanoscale distribution of supported cobalt particles used in Fischer-Tropsch catalysis. *J. Am. Chem. Soc.* **2014**, *136*, 7333–7340. [CrossRef] [PubMed]
20. den Breejen, J.P.; Sietsma, J.R.A.; Friedrich, H.; Bitter, J.H.; de Jong, K.P. Design of supported cobalt catalysts with maximum activity for the Fischer-Tropsch synthesis. *J. Catal.* **2010**, *270*, 146–152. [CrossRef]
21. Gorboletova, G.G.; Metlin, A.A. Standard Thermodynamic functions of $Co^{2+}$ complexation with glycine and L-histidine in aqueous solution. *J. Phys. Chem.* **2016**, *90*, 334–338. [CrossRef]
22. Sun, K.Q.; Marceau, E.; Che, M. Evolution of nickel speciation during preparation of $Ni-SiO_2$ catalysts: Effect of the number of chelating ligands in $[Ni(en)_x(H_2O)_{6-2x}]^{2+}$ precursor complexes. *Phys. Chem. Chem. Phys.* **2006**, *8*, 1731–1738. [CrossRef] [PubMed]
23. Ouyang, R.H.; Liu, J.X.; Li, W.X. Atomistic theory of ostwald ripening and disintegration of supported metal particles under reaction conditions. *J. Am. Chem. Soc.* **2013**, *135*, 1760–1771. [CrossRef] [PubMed]
24. Kistamurthy, D.; Saib, A.M.; Moodley, D.J.; Niemantsverdriet, J.W.; Weststrate, C.J. Ostwald ripening on a planar $Co/SiO_2$ catalyst exposed to model Fischer-Tropsch synthesis conditions. *J. Catal.* **2015**, *328*, 123–129. [CrossRef]
25. Hong, J.P.; Wang, B.; Xiao, G.Q.; Wang, N.; Zhang, Y.H.; Khodakov, A.Y.; Li, J.L. Tuning the metal-support interaction and enhancing the stability of titania-supported cobalt Fischer-Tropsch catalysts via carbon nitride coating. *ACS Catal.* **2020**, *10*, 5554–5566. [CrossRef]
26. Eschemann, T.O.; Jong, K.P.D. Deactivation behavior of $Co/TiO_2$ catalysts during Fischer-Tropsch synthesis. *ACS Catal.* **2015**, *5*, 3181–3188. [CrossRef]
27. Loosdrecht, J.V.D.; Ciobîcâ, I.M.; Gibson, P.; Govender, N.S.; Moodley, D.J.; Saib, A.M.; Weststrate, C.J.; Niemantsverdriet, J.W. Providing fundamental and applied insights into Fischer-Tropsch catalysis: Sasol-eindhoven university of technology collaboration. *ACS Catal.* **2016**, *6*, 3840–3855. [CrossRef]
28. Rodríguez-González, V.; Marceau, E.; Che, M.; Pepe, C. Influence of the morphology and impurities of $Ni(OH)_2$ on the synthesis of neutral Ni(II)-amino acid complexes. *J. Solid State Chem.* **2007**, *180*, 3469–3478. [CrossRef]
29. Rodríguez-González, V.; Marceau, E.; Beaunier, P.; Che, M.; Train, C. Stabilization of hexagonal close-packed metallic nickel for alumina-supported systems prepared from Ni(II) glycinate. *J. Solid State Chem.* **2007**, *180*, 22–30. [CrossRef]
30. Koizumi, N.; Mochizuki, T.; Yamada, M. Preparation of highly active catalysts for ultra-clean fuels. *Catal. Today* **2009**, *141*, 34–42. [CrossRef]
31. Reuel, R.C.; Bartholomew, C.H. The stoichiometries of $H_2$ and CO adsorptions on cobalt: Effects of support and preparation. *J. Catal.* **1984**, *85*, 63–77. [CrossRef]
32. Puskas, I.; Fleisch, T.H.; Kaduk, J.A.; Marshall, C.L.; Meyers, B.L.; Castagnola, M.J.; Indacochea, J.E. Novel aspects of the physical chemistry of $Co/SiO_2$ Fischer-Tropsch catalyst preparations. Cobalt oxide-induced silica migration during calcination of cobalt nitrate-impregnated high surface area silica. *Appl. Catal. A Gen.* **2007**, *316*, 197–206. [CrossRef]

33. Lü, B.Z.; Qi, W.J.; Luo, M.S.; Liu, Q.L.; Guo, L. Fischer-Tropsch synthesis: ZIF-8@ZIF-67-derived cobalt nanoparticle-embedded nanocage catalysts. *Ind. Eng. Chem. Res.* **2020**, *59*, 12352–12359. [CrossRef]
34. Jagadeesh, R.V.; Murugesan, K.; Alshammari, A.S.; Neumann, H.; Pohl, M.M.; Beller, M. MOF-derived cobalt nanoparticles catalyze a general synthesis of amines. *Science* **2017**, *358*, 326–332. [CrossRef]
35. Sun, Z.K.; Sun, B.; Qiao, M.H.; Wei, J.; Yue, Q.; Wang, C.; Deng, Y.H.; Kaliaguine, S.; Zhao, D.Y. A General chelate-assisted co-assembly to metallic nanoparticles incorporated ordered mesoporous carbon catalysts for Fischer-Tropsch synthesis. *J. Am. Chem. Soc.* **2012**, *134*, 17653–17660. [CrossRef]
36. Bezemer, G.L.; Bitter, J.H.; Kuipers, H.P.C.E.; Oosterbeek, H.; Holewijn, J.E.; Xu, X.; Kapteijn, F.; van Dillen, A.J.; de Jong, K.P. Cobalt particle size effects in the Fischer-Tropsch reaction studied with carbon nanofiber supported catalysts. *J. Am. Chem. Soc.* **2006**, *128*, 3956–3964. [CrossRef]
37. Breejen, J.P.D.; Radstake, P.B.; Bezemer, G.L.; Bitter, J.H.; Frøseth, V.; Holmen, A.; Jong, K.P.D. On the origin of the cobalt particle size effects in Fischer-Tropsch catalysis. *J. Am. Chem. Soc.* **2009**, *131*, 7197–7203. [CrossRef]